Damping and non-linearity of a levitating magnet in rotation above a superconductor

2014 New J. Phys. 16 075011

(http://iopscience.iop.org/1367-2630/16/7/075011)

New Journal of Physics
The open access journal at the forefront of physics
Deutsche Physikalische Gesellschaft DPG | IOP Institute of Physics

Damping and non-linearity of a levitating magnet in rotation above a superconductor

J Druge, C Jean, O Laurent, M-A Méasson and I Favero
Matériaux et Phénomenes Quantiques, Université Paris Diderot, CNRS UMR 7162, Sorbonne Paris Cité, 10 rue Alice Domon et Léonie Duquet, 75013 Paris, France
E-mail: marie-aude.measson@univ-paris-diderot.fr and ivan.favero@univ-paris-diderot.fr

Received 17 July 2013, revised 6 June 2014
Accepted for publication 6 June 2014
Published 17 July 2014
New Journal of Physics **16** (2014) 075011
doi:10.1088/1367-2630/16/7/075011

Abstract
We study the dissipation of moving magnets in levitation above a superconductor. The rotation motion is analyzed using optical tracking techniques. It displays a remarkable regularity together with long damping time up to several hours. The magnetic contribution to the damping is investigated in detail by comparing 14 distinct magnetic configurations and points towards amplitude-dependent dissipation mechanisms. The non-linear dynamics of the mechanical rotation motion is also revealed and described with an effective Duffing model. The magnetic mechanical damping is consistent with measured hysteretic cycles $M(H)$ that are discussed within a modified critical state model. The obtained picture of the coupling of levitating magnets to their environment sheds light on their potential as ultra-low dissipation mechanical oscillators for high precision physics.

Keywords: levitation, mechanical oscillator, superconductor, damping, non-linear, optomechanics

Mechanical oscillators with ultra-low dissipation find applications as frequency standards, as probes of minute forces (e.g., atomic force microscopy), or in signal processing, where they can serve as fine radio-frequency filters. At a basic science level, they received attention in the past for their impact in high precision physics and metrology [1, 2]. More recently, they have become a central subject for a whole community of physicists aiming at observing the quantum behavior of mesoscopic mechanical systems [3, 4]. This quest has seen impressive advances notably thanks to optomechanical systems [5–7] that use the concepts of coupling light and mechanical motion, possibly in the regime where the quantumness of the mechanics starts being tangible [8, 9]. In all these situations, low dissipation of the mechanical degree of freedom is required to protect it against quantum decoherence or classical fluctuations of its environment.

Sources of dissipation are manyfold, but one ubiquitous amongst mechanical systems is the anchoring (clamping) loss, which stems from the fact that the system is mechanically attached to a support. To circumvent this source of loss, one obvious solution is to levitate the mechanical system. If we disregard optical levitation [10–13], which restricts to nanoscopic mass objects, diamagnetic effects in superconductors (SCs) are the most established technique to levitate a macroscopic mass and hence isolate a mechanical oscillator from its support. Superconducting magnetic levitation has been extensively studied in the context of bearings for transportations [14], but surprisingly, the applications of these systems in high precision physics remains relatively scarce [15]. At the microscopic scale, the dissipation and decoherence of atoms trapped on top of superconducting surfaces has been investigated recently [18–21]. At the macroscopic scale, magnetic levitation was mentioned in early discussions of quantum effects in mechanical systems [2], and it has been the topic of recent theoretical works investigating quantum-control protocols [16, 17]. However, a gap remains between proposals and experiments when it comes to quantitative prediction of mechanical dissipation in magnetic levitating bodies. Despite a series of work focusing on the centre of mass motion of magnets above some superconductors [23], the motional damping of levitating macroscopic objects still calls for additional documentation, as a complete understanding and parameter-free modeling of underlying mechanisms is still lacking. There is, for example, no exhaustive picture of which ultimate level of dissipation such a levitating system could reach in a refined low-amplitude force sensing experiment or in the quantum regime. This paper is a first step to try to answer these questions. To that aim, we carry out simple but systematic experiments on one of the most ubiquitous systems: a magnet levitating over a high critical temperature (T_c) superconductor.

We employ commercial NdFeB sphere magnets (SMs)[1] with large coercivity of $\sim$900 kA m^{-1} of diameters varying between 5–26 mm and position them one after another over a high-T_c $Y_{1.65}Ba_2Cu_3O_{7-x}$ superconducting cylinder pad[2]. We use two types of superconductors in the experiments. The T_c is 90.5 K, and the critical current j_c is in the range of 20–40 kA cm^{-2} for both. The two types of superconductor differ in terms of levitation forces because of a difference in their grain structure. One is a 'melt-textured unseeded material' superconductor that traps lesser amount of field and will be referred to as 'soft anchoring' pad. The second is a 'melt-textured single-grain' superconductor that can trap a larger amount of magnetic field and will hence be named 'hard anchoring'. The soft or hard anchoring nature of the material is directly appreciable when manually moving the magnet trapped above the superconductor.

As illustrated in figure 1, the superconducting pad is kept at a low temperature below its T_c by contacting it with apiezon grease to a large copper cylinder immersed into a liquid nitrogen bath. In order to increase thermal inertia and stability of the set-up during hour-long measurements, a polystyrene box of very large liquid capacity is used as the bath and placed on

[1] From *Supermagnete*, spheres with a Ni-Cu-Ni-Cr coating.

[2] From *ATZ*, HTS YBCO elements, melt textured, unseeded material (soft anchoring, pad thickness 4 mm and diameter 40 mm) and melt textured, single grain (strong anchoring, pad thickness 6 mm and diameter 30 mm).

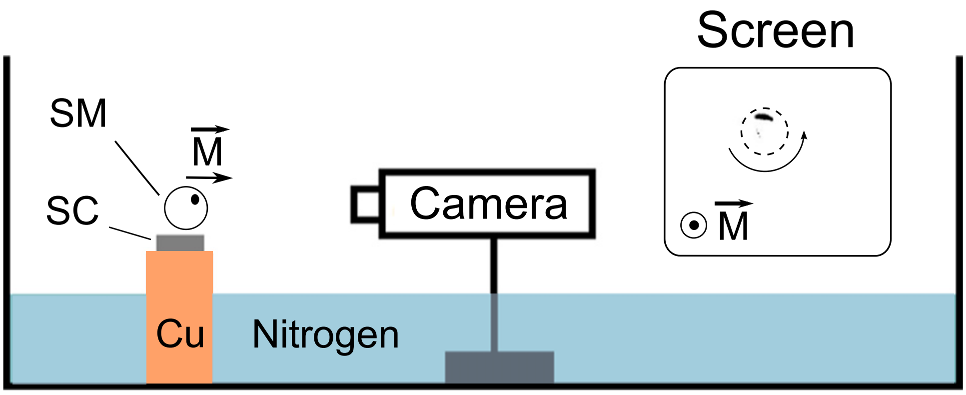

Figure 1. Schematics of the experiment. A spherical magnet (SM) levitates and experiences a rotational motion over a superconductor (SC) pad thermally connected to a copper (Cu) cylinder plunged into liquid nitrogen. $\vec{M}$ is the magnetic dipole moment of the magnet. Inset shows a typical video image after treatment with the mark spot (in black) within the rotating magnet boundaries (dashed circle).

a mechanically isolating bench. Air turbulence and convection are kept to a low level during measurements.

In this work, we focus on the rotation motion of the sphere magnet around its magnetic axis, because this motion presents a very low dissipation. Indeed, in the case of a perfectly homogeneous and spherical magnet, the magnetic configuration of the experiment is invariant upon rotation of the sphere around this axis. As a consequence, strictly no magnetic damping of the sphere rotation motion should occur. As we will see, even in a real and non-ideal experimental situation, this argument still holds to some extent, and very long damping times of hours can be observed for this rotation motion. Note that other types of motion involving millimeter scale displacements of the magnet centre of mass are systematically observed to damp rapidly in much less than a minute, and will hence not be considered here.

A video camera is positioned near the magnet to register its motion. The camera optical axis is superposed to the sphere magnetic axis defined by the magnetic dipole $\vec{M}$. In order to allow systematic data analysis of the motion, a black mark spot is drawn on the magnet, and a treatment of each video image is performed to increase its contrast. After treatment, a typical image displays the isolated black mark spot over a white background, where the magnet spherical boundary is hardly visible (see inset of figure 1). This strong contrast allows for each image to run an automated search of the mark spot barycenter, leading its radial coordinate (amplitude and phase) with respect to the centre of the spherical boundary. In a rotation around $\vec{M}$, the amplitude remains constant, and the motion is analyzed by registering the phase evolution upon time. In the following, we use this method to measure both rotation motion (with increasing phase upon time) and rotation-oscillation motion (with oscillating phase upon time). The observed motion damping is highly dependent on the orientation of the magnet dipole $\vec{M}$ with respect to the rest of the set-up, with a minimum damping consistently observed when the axis is horizontal to the pad plane. We therefore adopt this orientation for all reported experiments (figure 1). Second, the damping also depends on the height at which the magnet is levitating above the superconducting pad. Hence, in our experiments we employ a constant levitation height defined as being the distance between the upper pad plane and the bottom of

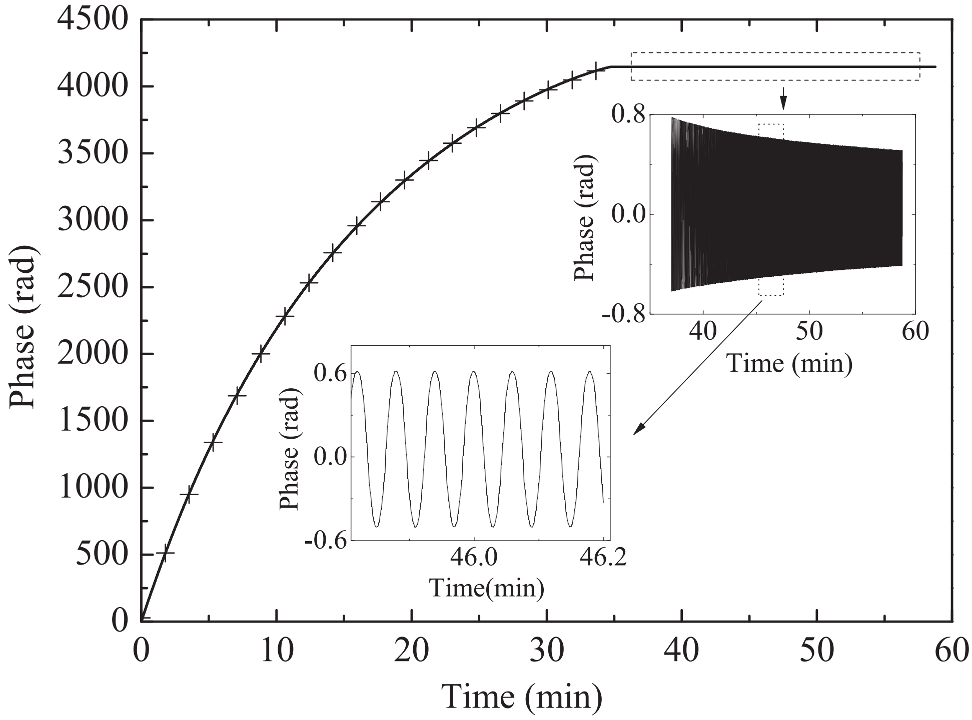

Figure 2. Typical rotation motion of a levitating sphere magnet. Time evolution of the phase for a sphere magnet of diameter 12.7 mm levitating over a soft anchoring superconductor. Solid lines are employed for experimental data in order to illustrate their remarkable regularity, while cross symbols are employed for the exponential fit. The top-right inset is a first close-up on the rotation-oscillation motion, where the envelope of the phase trace is apparent. The lower inset is a second close-up focusing on the time oscillation, where a time period of a few seconds is visible.

the sphere. To that purpose, every sphere magnet is first deposited at room temperature on an interstitial Teflon element of fixed height of about 12 mm sitting on the pad. The system is then cooled in a field cooled process and the interstitial element removed before setting the levitating magnet in rotation.

Figure 2 shows a typical measurement of the phase upon time after the levitating sphere magnet has been put in rotation manually. A rotation motion first lasts about 35 min before reaching a plateau where the phase oscillates upon time, corresponding to a rotation-oscillation motion, as seen clearly in the lower inset. During the first rotation part, the rotation speed progressively decreases, and the phase is very accurately described by a time exponential function typical of a linear damping model. In the second part where rotation-oscillation takes place, the oscillation amplitude is itself damped in a time exponential manner as seen in the top right inset of figure 2. This behavior is again reminiscent of the harmonic oscillator model with linear damping. It is worth noting that the rotation motion of some magnets is observed to last for more than 8 h, reaching the limit of our ability to measure it reliably. In the following, we study in details the origin of the observed damping.

First, as our experiments are run under ambient conditions, the surrounding air can be a source a friction for the rotation motion. However, we do not expect air to produce a restoring torque, while the existence of such torque is implied by the observation of oscillatory rotation motion in the experiments. The forces responsible for this torque act at a distance on the spheres

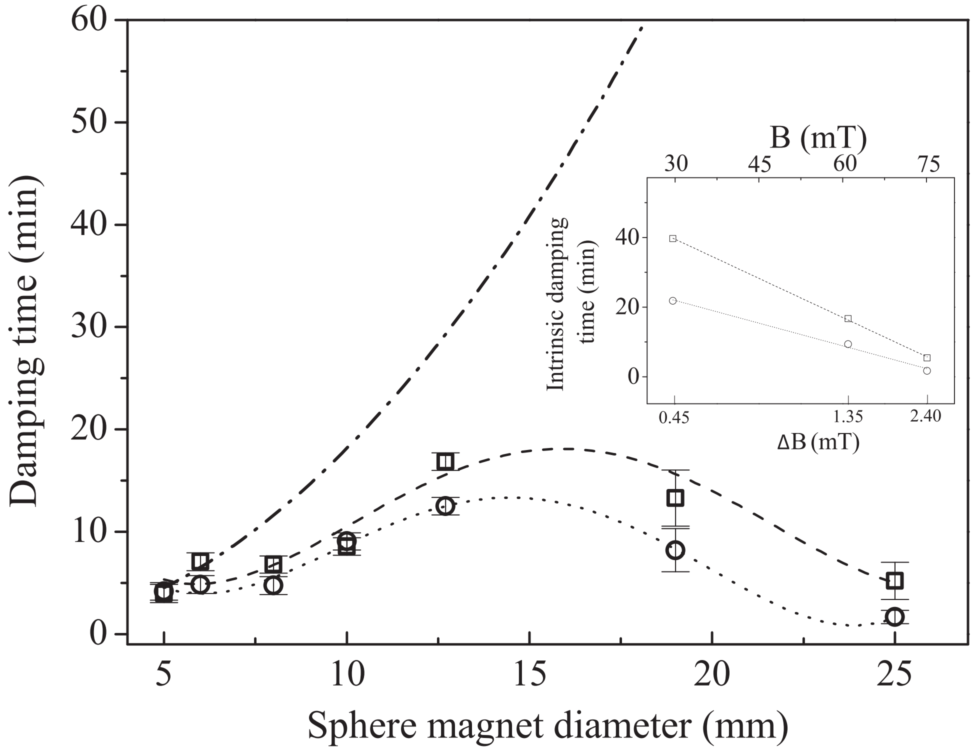

Figure 3. Damping of the rotation motion for different magnetic configurations. The main plot shows the total damping time as a function of the sphere diameter for the soft anchoring (squares) and hard anchoring (circles) superconductor. Dashed lines are guides to the eye. The dashed-dotted line is a calculation of the damping time induced by air viscosity. The inset shows the intrinsic damping time as a function of the magnetic field B on the top surface of the superconducting pad (see text for details), showing the role of magnetic effects in the damping. ΔB is the amplitude (peak to peak) of the inhomogeneity of the magnetic field applied by the magnetic sphere on the top surface of the superconductor pad (see appendix).

and may be magnetic in nature, contradicting the picture of a rotation invariance of the sphere around its magnetic axis. The rotation invariance is also questioned by our independent observation of an inhomogeneous magnetic field as one rotates the magnetic sphere, which we could reveal in the orientation of iron filings or by using a magnetic foil. We conclude that the employed magnetic spheres are not perfectly rotation-invariant around their magnetic axes and that a strictly null magnetic damping of the rotation cannot be expected. In the appendix, we show a more complete characterization of these magnetic inhomogeneities by a macroscopic Hall probe.

To study the role of magnetic effects in the damping of the rotation motion, we now vary both the magnetic configuration of the spheres and their magnetic environment. To that aim, we vary the diameter of the spheres and employ the two different types of superconductor introduced above, one with a large trapped magnetic field (hard anchoring) and one with a lower trapped field (soft anchoring). In each configuration, we systematically measure the rotation damping during the first part of the motion, where the phase decays exponentially.

Figure 3 reports the measured damping time as a function of the sphere diameter, exploring 14 different configurations in total. The open square symbols correspond to the superconductor with soft anchoring; the circle symbols correspond to the superconductor with hard anchoring. The dash-dotted line is a theoretical value for the air damping contribution, which is obtained using the Stokes model for a rotating sphere in a non-turbulent incompressible fluid [23]. In figure 3 the damping measured for the spheres of small diameter (5 and 6 mm) seem to be explained by air damping, but as the magnet diameter increases, there is a strong departure from this contribution. Air damping has a negligible contribution on the spheres of large diameter like 12.7, 18 and 26 mm. On these spheres, the measured damping time varies when using the hard or the soft anchoring superconductor, showing that the magnetic properties of the superconductor play a key role in the rotation dynamics. To reveal even more clearly these magnetic effects, we plot in the inset of figure 3 the damping time as a function of the sphere magnetic field on the superconductor pad B and of its inhomogeneity ΔB. To obtain these data, we measure the magnetic field of the sphere alone (with no superconductor) with a Teslameter at a distance from the sphere corresponding to the levitation height, on the magnetic equatorial line where the pad lies in the levitating configuration (see appendix). The theoretical air damping contribution is removed from the inset data to make the 'intrinsic damping time' directly appear. The plot clearly reveals that the 'intrinsic damping' increases as the magnetic field on the pad increases, and tends to be larger for the 'hard anchoring' pad as compared to the 'soft' (see appendix for a discussion of this trend).

These observations points towards the role of vortices in the damping of rotation motion. Indeed, the larger the magnetic field applied by the magnet to the superconductor pad, the larger the amount of vortices accommodated in the pad. The vortices are known to be responsible for the rigidity of the superconducting levitation configuration, but this rigidity is also accompanied by a dissipative contribution. In early experiments a magnet was displaced above a superconductor and a lossy hysteric was observed that revealed energy dissipation as vortices move in the superconductor [24–26]. In our experiments, because the sphere magnet is not perfectly symmetrical (see appendix), the rotation motion modulates the stray magnetic field on the pad with an amplitude ΔB and consequently the vortices configuration in the superconductor, producing dissipation. Our measurements, notably the inset of figure 3, confirm that dissipation of the rotation motion grows with ΔB. In the rotation-oscillation case, where the amplitude of rotation is smaller, the field variation experienced by the superconductor is also smaller, such that a lesser amount of dissipation is expected. This picture suggests a mechanical damping that depends on the motion amplitude [22]. There has been a recent strong interest in such non-linear damping mechanisms in nanoscale mechanical systems, which would make them depart from the conventional damped harmonic oscillator behavior [28, 29]. In the following we will not specifically focus on the linear and non-linear aspects of the damping but will show on a more general foot that strong non-linearities are indeed present in the dynamical behavior of rotating magnets in levitation above superconductors.

Figure 4(a) shows the phase time evolution of a 19 mm diameter sphere magnet in rotation-oscillation above a strong anchoring superconductor. The evolution is qualitatively different from the one shown in figure 2, in that several abrupt changes are now visible in the envelope evolution. These abrupt changes cannot be explained by a harmonic oscillator model and convey the picture of an oscillation motion within multiple adjacent potential wells. As the mechanical energy dissipates upon time, the system progressively restricts its motion to fewer wells until it resides within a single of these, where the mechanical energy finishes to be dissipated. Figure 4(b) shows such final evolution in the last well for a 26 mm diameter sphere levitating over the same superconductor. Even in this case, where a unique well is involved, the phase evolution reveals a

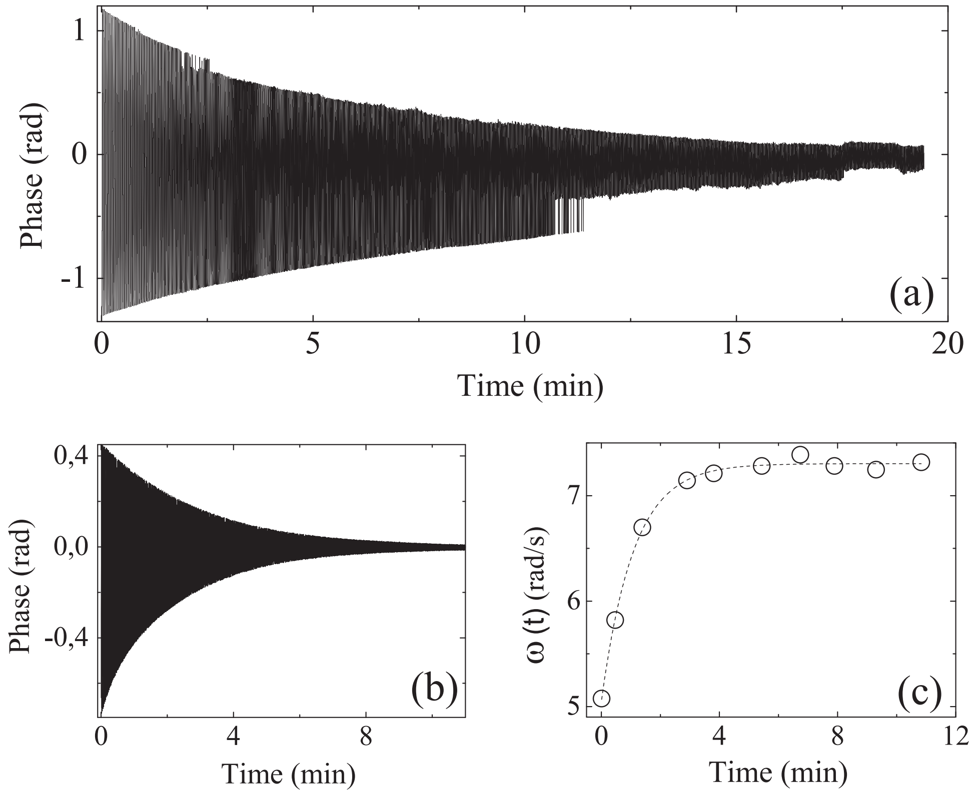

Figure 4. Non-linearities in the rotation of magnets levitating above a superconductor. (a) The time evolution of the phase of a rotation-oscillation motion, in a case where the envelope experiences several abrupt changes upon time. (b) The final evolution after the last abrupt change, displaying an asymmetry of the envelope. (c) The corresponding time evolution of the instantaneous angular frequency. The open circles are data, and the dashed line is the fit function predicted by the effective Duffing model (see text for details).

non-linearity. The envelope amplitude is strongly asymmetric with respect to the zero axis, implying an anharmonicity in the related trapping potential. Indeed, the harmonic oscillator with linear damping predicts a symmetrical envelope and a constant angular frequency of the oscillation upon time. In our experiments, the potential anharmonicity is also witnessed by the time-evolution of the angular frequency $\omega(t)$, which is reported in figure 4(c) for the damped motion of figure 4(b). Each value of $\omega(t)$ is obtained by analyzing the oscillation motion over 10 oscillations. The measured angular frequency is not constant but follows an exponential time evolution. We analyze this behavior by adopting a simple Duffing model with damping:

$$\ddot{\Theta}(t) + \lambda\dot{\Theta}(t) + \omega_0^2\Theta(t) + B\omega_0^2\Theta^3(t) = 0, \quad (1)$$

with B < 0 as the Duffing coefficient. To deal with this non-linear equation, we propose a mathematical ansatz inspired by our experimental results. We inject the following expression for the phase evolution:

$$\Theta(t) = A\exp\left(-\frac{\lambda t}{2}\right)\cos(\omega(t)\,t) \quad (2)$$

in the equation and try to solve for $\omega(t)$. To that aim, we make several simplifications, which are again justified by our experimental results. These simplifications, valid for any time t of our experimental analysis, are the following:

$$\lambda \ll \omega(t),\ \dot{\omega}(t)\,t \ll \omega(t),\ \ddot{\omega}(t)\,t \ll \dot{\omega}(t), \tag{3}$$

from which we obtain a simplified equation for the time evolution of $\omega(t)$, once the terms in $\lambda\omega$ are disregarded with respect to the terms in ω^2:

$$\frac{\omega(t)^2}{\omega_0^2} = 1 + BA^2 \exp(-\lambda t) \cos^2(\omega(t)\,t), \tag{4}$$

At this stage, we now integrate over a period of the cosine, considering that $\omega(t)$ does not evolve at this time scale. This last step allows to smooth out the rapid time evolution and obtain the correct slow evolution of $\omega(t)$ in the form of:

$$\omega(t)^2 = \omega_0^2\left(1 + \frac{BA^2}{2}\exp(-\lambda t)\right). \tag{5}$$

This is the form employed now to obtain the fit in figure 4(c), with λ of $0.82\,\mathrm{min}^{-1}$ extracted from the envelope evolution measured in figure 4(b), and $B = -1.6$ taken as an adjustable parameter. The agreement with experimental data is very satisfactory, considering the simplified mathematical solving of our non-linear model. This agreement further confirms the non-linear dynamics of magnets levitating above superconductors, an aspect that would need to be considered for high precision experiments.

In this work, we have focused on the rotation motion of millimeter-sized magnetic spheres. The studied motion has a very large amplitude. During hour-long rotation levitating above a superconductor, a point on the sphere surface would typically be displaced over at least several tens of meters of curve coordinate. On the other hand, the smallest amplitude of motion that can be detected in the present experiments is commensurate with the mark spot size, on the order of the millimeter. This size scale is still close to the magnet's dimensions, a scale at which the mechanical motion is not expected to be governed by linear couplings. This is put under light in our experiments, where a non-linear dynamics is revealed in several different aspects of the rotation motion. We also measured the mechanical damping associated to the dissipative pinning of vortices in the superconductor, which also lends itself to non-linearities [14, 26].

In the appendix, we show that the standard Bean critical state model does not allow a proper description of the observed damping and leads to wrong quantitative predictions for our experiments. The magnetic damping is better discussed within the modified critical state model of Irie and Yamafuji [26, 27], which also implies non-linear damping. For magnetically levitating systems above superconductors, the question of the dissipation at very low amplitude, in such range that the vortices can rest on their pinning centres on a whole cycle, is still open [30]. As discussed by Campbell [31], the linear response of a superconductor to a low amplitude field is not correctly described by a critical state model. The implications of this harmonic regime for the mechanical damping of levitating bodies remains to be investigated. For all these reasons, there is a clear need for measuring the rotation of levitating sphere magnets in a purely linear regime, where best performances in terms of a precision oscillator are expected. Such a regime is currently not accessible to our observation. This situation calls for another level of sensitivity in our measurements to resolve directly the Brownian mechanical motion of these levitating systems and reach a situation where mechanical energy originates merely from

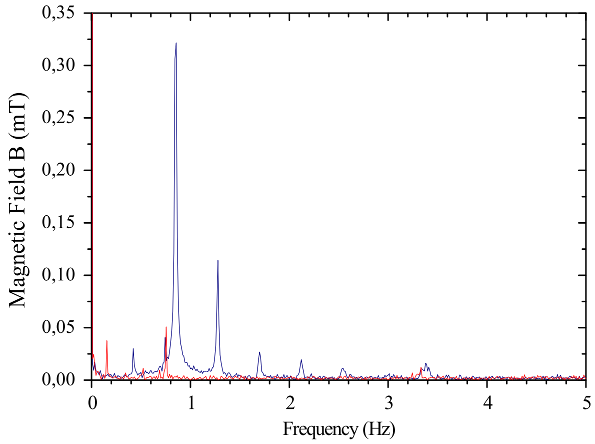

Figure A1. Fast Fourier transform (FFT) of the measured field B when rotating the sphere magnet (26 mm diameter) around its magnetic axis with a frequency of about 0.85 Hz (blue curve) and for the sphere 'at rest' (red curve).

fluctuations. Optomechanical cavity detection techniques are a natural candidate for reaching this regime and will open a route for the optomechanics of macroscopic levitating objects.

Acknowledgments

We thank Julien Gabelli for discussions on the physics of magnetic levitation. We acknowledge Brigitte Leridon for her help in the magnetization measurements. This work has been supported by a grant from the region Ile de France. We thank Professor Kordyuk for helpful discussion and the ATZ company for providing detailed informations on the superconducting materials.

Appendix A: Sphere magnet inhomogeneity

We have employed a magnetic probe (macroscopic Hall probe) to sense the magnetic stray field of the sphere magnets. The probe was positioned at a distance to the sphere that equalled the levitation height of the magnet above the superconducting pad. The orientation of the probe was chosen in order to evaluate the maximum magnetic field penetrating in the superconductor during the field-cooled process before levitation. The measurement of the stray field was carried out when rotating the sphere magnet around its magnetic axis or with the sphere at rest.

The time trace of the measured field, with the sphere rotating, revealed rather regular time behavior, also apparent in the fast Fourier transform (FFT), where a limited number of harmonics was observed. Most often one single harmonic, positioned in the 3–5 Hz window, dominated the spectrum. This harmonic corresponded to the rotation frequency, which was also independently measured with a timer. Figure A1 plots an example of such an FFT spectrum, acquired for a 26 mm diameter sphere magnet, showing the magnetic field amplitude as a function of frequency. The blue curve is for the sphere rotating with a frequency of about 0.85 Hz; the red curve is for the sphere 'at rest' meaning that no rotational motion is visible to the eye. The fact that one harmonic at the rotation frequency dominates the spectrum indicates that the heterogeneity of the stray field is at first order of description approximated by a $\cos(\theta)$ profile, where θ is the phase of the rotational motion (one field maximum in one rotation period

Table A1. Peak-to-peak variation (ΔB) of the magnetic field (as inferred from the time trace measurement) when the sphere rotates. Mean field B and corresponding ΔB/B. Measurements are carried out on spheres of varying diameter, with an average of 4 measurements per diameter. Coercivity field of the magnets are also reported.

Sphere diameter (mm)	ΔB(mT)	B(mT)	ΔB/B (%)	H_c (kA/m)
8	0.2 ± 0.1	11.8 ± 0.1	1.9 ± 0.8	$860 - 915$
12.7	0.45 ± 0.03	29.6 ± 0.3	1.5 ± 0.1	$860 - 955$
26	2.4 ± 0.1	75.1 ± 0.3	3.2 ± 0.3	$860 - 915$

in this first order description). The peak-to-peak variation of the magnetic field (as inferred from the time trace measurement) is of 2.4 mT when the sphere rotates, corresponding to a value of $\Delta H/H$ of 3.2% (the mean field is 75.1 $\pm$ 0.3 mT). When the sphere is 'at rest' the peak-to-peak variation is 0.3 mT. Such measurements were carried out on spheres of varying diameter, with an average of 4 measurements per diameter. The results are summarized in the following table A1, together with the coercivity of the magnets.

The table shows an average $\Delta H/H$ in the few percents upon one 2π rotation. Regarding the coercivity of the magnets in table A1, it remains in the Tesla range when expressed in the dimension of a magnetic field. This value is several orders of magnitude larger than the maximum stray field that we measured, which itself is an upper bound of the field that could back-act on the magnet during levitation. Magnetic hysteresis in the sphere magnet can thus be safely ruled out in our experiments. We have also evaluated the maximum eddy current losses (for the largest sphere) and checked that they can be neglected in our set of investigations.

Appendix B: Discussion of results within critical state models

Bean critical state model

Within the Bean critical state model [32], losses are produced by the hysteric response of the system when immersed in an external time-varying magnetic field. A formula can be obtained for the dissipated power per cycle in some specific geometries and allows discussing qualitative behaviors and sometimes even quantitative aspects. In this model, the dissipated power scales with the inverse of j_c such that a high j_c (sometimes referred to as a hard pinning) would dissipate less than a small j_c (sometimes referred to as a soft pinning). In our experiments, we employ two types of superconductors: 'soft anchoring' and 'hard anchoring' with a similar critical current value j_c of 20-40 kA cm^{-2}. The T_c is 90.5 K for both superconductors, specified by the material provider and checked directly in a measurement of the magnetization as a function of temperature. The difference between the two superconductors in terms of levitation forces (one strong and one weak) is due to a different maximal trapped field resulting from a difference in the grain structure. The first superconductor is a 'melt-textured, unseeded material' superconductor (smaller grain size and multi-domain structure) that traps a lesser amount of field. The second is a 'melt-textured, single-grain' superconductor (a mono-domain of larger size) that can trap a larger amount of magnetic field. A complete discussion of these different materials and their impact on levitation forces can be found in Jin *et al* [33]. As shown in this reference, the area within the hysteresis curve of a single-grain material can be larger than for a multi-domain material, such that the associated dissipation is also larger. In this sense a 'hard anchoring' superconductor can sometimes dissipate more than a 'soft-anchoring', showing that arguments coming solely from the Bean model, if not discussing structural aspects of the material, do not explain all observed trends.

Still, even if the Bean model does not allow complete understanding, we attempted to employ it in our case. The Bean formula on dissipated energy E per cycle is based on an assumption of a time-varying magnetic field parallel to the surface of a semi-infinite superconductor $E = 2/3\pi R^2\mu_0 \Delta H^3/j_c$, considering that the volume in which dissipation takes place is $\pi R^2 W$ (surface projection of the sphere πR^2 and thickness of the pad sample W). We employed this formula to evaluate dissipation in the data of figures 4(b) and (c) and found the energy dissipated per hysteretic cycle to be $4 \cdot 10^{-11}$ J when using $j_c = 30\ \mathrm{kA\,cm^{-2}}$, $R = 13$ mm, and $\Delta B = (2.4/2\pi)$ mT for the rotation motion of figure 4(c), where the amplitude of rotation at time $t = 0$ is of 1 radian instead of 2π. This value of $4 \cdot 10^{-11}$ J is evaluated for the motion of figure 4(c) at time $t = 0$. Within the Bean model, the area within the hysteretic curve decreases as the amplitude of field variation decreases. At time $t = 4$ min, the amplitude of rotation is of 0.25 radian, leading to a reduction of a factor of 64 of the dissipated power per cycle to $6 \cdot 10^{-13}$ J. On average, the Bean model predicts a dissipated power per cycle of about 10^{-12} J in the data of figures 4(b) and (c). In our manuscript, we interpreted the data of figure 4 within a Duffing model with linear damping, which proved efficient to describe the observed non-linearity, the trends in the damping and the evolution of the rotation angular frequency. Let us now discuss the energy dissipated per cycle within this model. In the data of figures 4(b) and (c), the energy dissipated in the first cycle ($t \approx 0$) amounts to $\lambda/\omega_0 \times 2\pi \times$ Stored Energy $= \lambda/\omega_0 \times 2\pi/5 \times mR^2\omega_0^2 A^2 = 10^{-6}$ J using the values for A, with λ and ω_0 obtained from the fit by equation (4) of the manuscript. Similarly, the energy dissipated in a cycle at time $t = 4$ min amounts to $\lambda/\omega\,(t = 4\text{ min}) \times 2\pi/5 \times mR^2\omega^2\,(t = 4\text{ min})A^2 \times \exp(-\lambda \cdot 4\text{ min}) = 6 \cdot 10^{-8} J$. On average, we obtain an energy dissipated per cycle of 10^{-7} J. In conclusion, the Bean model underestimates the energy dissipated per cycle by about 5 orders of magnitude for the rotation-oscillation data of figures 4(b) and (c).

In the same line, we estimated whether the damping measured in figure 2 (rotation) could be compared to expectations from the Bean model. We note here that the measured exponential decay of the phase cannot be directly obtained from the Bean model that implies a constant dissipated power per cycle. However, the dissipated power per cycle expected from the Bean model can still be compared to experimental data, and a dissipation time t_d can be computed. We obtain $t_d = 3Tj_c/\omega\mu_0\Delta H^2 R^2$, considering that all of the kinetic energy T is lost after a time t_d. We have $T = 1/2 \times 2/5 \times mR^2\omega_0^2$, and we approximate $\omega = \omega_0$ to obtain $t_d = 3/5\, m\omega_0 j_c/\mu_0\Delta H^3$. In figure 2 we have $\omega_0 = 4$ radian $\mathrm{s^{-1}}$; the sphere is 12.7 mm in diameter with a mass of 8.8 g. $\Delta H = \Delta B/\mu_0$ with $\Delta B = 0.45$ mT for that sphere, as indicated in table A1. The numerical illustration gives $t_d = 1803$ min, to be compared to 17 min found from the exponential fit of experimental data in figure 2. Here again for the rotation motion, the standard Bean model underestimates the damping by several orders of magnitude.

Modified critical state model

To understand the gap between the standard Bean critical state model and our experimental observations, we carried out additional magnetic hysteretic cycle measurements (M versus H) at 77 K. These measurements employed an MPMS Squid Magnetometer set-up (Magnetic Properties Measurement System, from Quantum Design company). We measured both the 'soft anchoring'

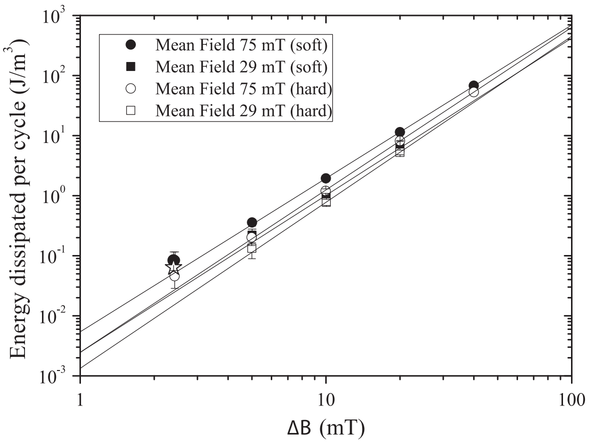

Figure B1. Energy dissipated by cycle, per unit volume, as a function of the amplitude of the field variation, and for different field mean values, for both 'soft anchoring' and 'hard anchoring' superconducting material extracted from magnetic hysteretic cycles measurements (M versus H) at 77 K in an MPMS Squid Magnetometer set-up.

and 'hard anchoring' superconducting material in a time-varying external magnetic field. The field varied around a mean value in the few tens of mT, close to the field amplitude applied on the superconductor in the levitation experiments. The amplitude of the field variation was tuned from a few mT, close to its value during levitation, to a few tens of mT. The area comprised within the M (H) hysteretic curve was extracted from each measurement and converted into energy dissipated per hysteretic cycle. Figure B1 shows the resulting energy dissipated by cycle, per unit volume, as a function of the amplitude of the field variation, and for different field mean values, for both superconductors. The logarithmic plot reveals a scaling of the dissipated power with ΔH with an exponent of 2.55–2.62 (soft anchoring) and 2.70–2.76 (hard anchoring), when the standard Bean model predicts an exponent of 3. These measurements indicate that the critical state model must be modified to account for the magnetic hysteretic behavior of the two superconductors employed in our levitation experiments.

References [26, 27] propose a formula for the energy dissipated during a hysteretic cycle per unit volume for a modified version of the critical state model (Irie–Yamafuji model) $E = 2/3 \cdot (2 - \gamma) \cdot \mu_0 \Delta H^{4-\gamma} / \left(j_c W\right)^{2-\gamma}$, where γ is a free parameter that usually varies in the literature between 0–1.4. $\gamma = 1$ corresponds to the standard Bean model. For the energy dissipated, the data of figure B1 indicate a scaling value γ as a function of ΔH between 1.23–1.42, with a pre-factor that is let free in the fits.

We now compare the findings of these MPMS data to the levitation experimental data. The comparison can be done on a sphere magnet of diameter 26 mm in rotation motion, in the same manner as above. The experiments measuring the rotation phase upon time lead us to evaluate an energy dissipated per cycle of $1.3 \cdot 10^{-7}$ J. This value, normalized to the dissipation volume $W\pi R^2$, has been reported for comparison in figure B1 by a star symbol, showing a reasonable agreement with values obtained by MPMS. Figure B1 also shows an energy dissipated by magnetic cycle per unit volume that is about the same (within a factor of two) for the 'soft anchoring' superconductor and the 'hard anchoring'. In the levitation experiments, the 'hard anchoring' superconductor pad had a thickness W of 6 mm, against 4 mm for the 'soft anchoring' pad. In the modified critical state model (Irie–Yamafuji model), the volume loss scales inversely with W with a factor $2 - \gamma$. Once multiplied by a loss volume of $W\pi R^2$, the scaling with W becomes $\gamma - 1$, which amounts to about

0.35 for our superconducting materials. In this case, the difference of thickness in the pads used in the levitation experiments produces a damping 15% larger for the hard anchoring pad when compared to the soft anchoring one. In this case, a mere geometric effect produces more damping of rotation motion when using the 'hard anchoring' superconductor, contrary to what would be usually expected in the Bean model picture.

In conclusion, the Irie–Yamafuji model (modified critical state model) allows a description of the magnetic behavior of the superconductors employed in our experiments. The hysteretic losses measured by a squid magnetometer reproduce the order of magnitude of the damping observed during levitating rotational motion. A complete agreement of the model to our data is beyond the scope of this work, as it would involve geometrical factors that are difficult to compute (finite size of the superconductor pad and spherical geometry of the magnet). For example, the 26 mm diameter sphere is commensurate to the pad diameter (30 mm for the 'hard' superconductor and 40 mm for the 'soft'). Additionally the sphere magnet stray field is not strictly described by a single spatial component cos (θ), when our simplified modeling relies on this assumption. Still, the findings reported in these appendixes strongly point toward magnetic losses in the levitation being governed by the physics of an Irie–Yamafuji model.

References

[1] Braginsky V B and Manukin A B 1977 *Measurement of Weak Forces in Physics Experiments* (Chicago, IL: University of Chicago Press)
[2] Braginsky V B, Mitrofanov V P and Panov V I 1985 *Systems with Small Dissipation* (Chicago, IL: University of Chicago Press)
[3] O'Connell A D *et al* 2010 *Nature* **464** 697
[4] Braginsky V B and Khalili F Y 1992 *Quantum Measurement* (Cambridge: Cambridge University Press)
[5] Favero I and Karrai K 2009 *Nat. Photon.* **3** 201
[6] Marquardt F and Girvin S 2009 *Physics* **2** 40
[7] Aspelmeyer M, Gröblacher S, Hammerer K and Kiesel N 2010 *J. Opt. Soc. Am.* B **27** 189–97
[8] Teufel J D, Donner T, Li D, Harlow J W, Allman M S, Cicak K, Sirois A J, Whittaker J D, Lehnert K J and Simmonds K W 2011 *Nature* **475** 359
[9] Chan J, Mayer Alegre T P, Safavi-Naeini A H, Hill J T, Krause A, Gröblacher S, Aspelmeyer M and Painter O 2011 *Nature* **478** 89
[10] Ashkin A 1970 *Phys. Rev. Lett.* **24** 156
[11] Barker P F and Shneider M N 2010 *Phys. Rev.* A **81** 023826
[12] Chang D E, Regal C A, Pappb S B, Wilson D J, Yeb J, Painter O, Kimble H J and Zoller P 2010 *Proc. Natl Acad. Sci. USA* **4107** 1005
[13] Romero-Isart O, Juan M L, Quidant R and Cirac J I 2010 *New J. Phys.* **12** 033015
[14] Moon F C 1994 *Superconducting Levitation: Applications to Bearing and Magnetic Transportation* (Weinheim: Wiley VCH)
[15] Prothero W A and Goodkind J M 1968 *Rev. Sci. Instrum.* **39** 1257
[16] Romero-Isart O, Clemente L, Navau C, Sanchez A and Cirac J I 2012 *Phys. Rev. Lett.* **109** 147205
[17] Cirio M, Brennen G K and Twamley T 2012 *Phys. Rev. Lett.* **109** 147206
[18] Hufnagel C, Tetsuya M and Shimizu F 2009 *Phys. Rev.* A **79** 053641
[19] Kasch B, Hattermann H, Cano D, Judd T E, Scheel S, Zimmermann C, Kleiner R, Koelle D and Fortágh J 2010 *New J. Phys.* **12** 065024
[20] Nogues G, Roux C, Nirrengarten T, Lupaşcu A, Emmert A, Brune M, Raimond J-M, Harroche S, Plaçais B and Greffet J-J 2009 *Europhys. Lett.* **87** 13002

[21] Fruchtman A and Horovitz B 2012 *Europhys. Lett.* **99** 53002
[22] Kordyuk A A and Nemoshkalenko V V 2003 *J. Low Temp. Phys.* **130** 207
[23] Landau L D and Lifshitz E M 1987 *Fluid Mechanics* (Oxford: Butterworth-Heinemann)
[24] Moon F C, Yanoviak M M and Ware R 1988 *Appl. Phys. Lett.* **52** 1534
[25] Hikihara T and Moon F C 1995 *Physica* C **250** 121
[26] Matsushita T 2007 *Flux Pinning in Superconductors* (Berlin: Springer)
[27] Irie F and Yamafuji K 1967 *J. Phys. Soc. Jpn* **23** 255
[28] Eichler A, Moser J, Chaste J, Zdrojek M, Wilson-Rae I and Bachtold A 2008 *Nat. Nanotechnol.* **6** 339
[29] Lifshitz R and Cross M C 2008 *Reviews of Nonlinear Dynamics and Complexity* vol 1 (Weinheim: Wiley-VCH) 2008
[30] van der Beck C J, Geshkenbein V B and Vinokur V M 1993 *Phys. Rev.* B **48** 3393
[31] Campbell A M 1969 *J. Phys. C: Solid State Phys.* **2** 1492
[32] Bean C P 1964 *Rev. Mod. Phys.* **36** 31
[33] Jin S, Sherwood R C, Gyorgy E M, Tiefel T H, van Dover R B, Nakahara S, Schneemeyer L F, Fastnacht R A and Davis M E 1989 *Appl. Phys. Lett.* **54** 584